Letter

Isotope-selective strong-field ionization of semiheavy water

A. J. Howard [1,2] M. Britton,[3] Z. L. Streeter,[4] C. Cheng,[2,5] R. R. Lucchese [6] C. W. McCurdy,[4,6] and P. H. Bucksbaum [1,2,3,5,*]

[1]Department of Applied Physics, Stanford University, Stanford, California 94305, USA
[2]Stanford PULSE Institute, SLAC National Accelerator Laboratory, Menlo Park, California 94025, USA
[3]Linac Coherent Light Source, SLAC National Accelerator Laboratory, Menlo Park, California 94025, USA
[4]Department of Chemistry, University of California, Davis, Davis, California 95616, USA
[5]Department of Physics, Stanford University, Stanford, California 94305, USA
[6]Chemical Sciences Division, Lawrence Berkeley National Laboratory, Berkeley, California 94720, USA

(Received 16 August 2024; accepted 12 February 2025; published 10 March 2025)

Semiheavy water (HOD) is one of the simplest molecules in which the bonds are labeled by isotope. We demonstrate that a pair of intense few-femtosecond infrared laser pulses can be used to selectively tunnel ionize along one of the two bonds. The first pulse doubly ionizes HOD, inducing rapid bond stretching and unbending. Femtoseconds later, the second pulse arrives and further ionization is selectively enhanced along the OH bond. These conclusions arise from 3D time-resolved measurements of H^+, D^+, and O^+ momenta following triple ionization.

DOI: 10.1103/PhysRevResearch.7.L012062

All chemical processes are mediated by the interatomic motion of electronic charge. New strategies to view and control the motion of electrons in molecules are improving our understanding of the earliest stages of chemical change [1–4]. Atomic-site-selective photoionization is one such method which has been indispensable for studies of charge migration and charge transfer [5–7]. XUV pulses from high harmonics and x-ray pulses from free electron lasers have both been used for site-selective ionization [8–11]. Here we demonstrate that the strong-field phenomenon of enhanced ionization (EI) driven by intense ultrashort infrared (IR) lasers is also atomic-site selective. In this case, the selectivity depends on atomic mass, such that isotopic substitution can be used to remove electrons from selected bonds.

Ultrashort IR lasers are often used to image nuclear dynamics in light molecules via laser-induced Coulomb explosion imaging (CEI) [12–15]. By this method, nuclear geometry is deduced from the ion fragment momenta following non-site-selective multiple ionization [16,17]. CEI works well in the limit of ultrashort few-femtosecond pulses because they can multiply ionize before the molecular structure changes [18–21]. If multiple ionization is performed sequentially and not instantaneously, the atoms in a molecule will start to move before Coulomb explosion. Site-selective EI may occur in this circumstance, due to distortions of the electrostatic potential created by nuclear motion and seen by certain bound electrons. EI has been observed in many small molecules to date, including H_2/D_2 [22–28], H_2O/D_2O [18,29–31], CO_2 [32–34], and C_2H_2 [35–37]. In each case, EI occurs when a bond stretches to a critical length and aligns with the laser polarization. The phenomenon thus depends on atomic motion, the speed of which changes with atomic mass. Therefore, when inducing EI in a hydrogen-containing molecule that has been selectively deuterated, ionization will be favored along different bonds at different times. By choosing to ionize at a particular time, we can achieve "isotope-selective" strong-field ionization (SFI), in which the tunneling of an electron primarily occurs along a particular bond that has been tagged by a particular isotope.

Isotopic labeling is a common technique in chemistry to tag otherwise indistinguishable atoms within molecules in order to track their evolution through a chemical process [38–40]. Semiheavy water (HOD) is one of the simplest products. Isotopic substitution does not alter the ground-state electronic structure, but can alter the ionization-driven nuclear dynamics such that SFI becomes atomic-site selective. To demonstrate this effect, we compare the fragmentation patterns of strong-field ionized H_2O, HOD, and D_2O.

A pair of cross-polarized 6-fs 750-nm pulses with equal peak intensity ($I_0 = 1 \times 10^{15}$ W/cm^2) sequentially ionize each target molecule. Two electrons are removed by the "pump" pulse. The dication evolves for a time Δt. A "probe" pulse then removes a third electron. The trication rapidly Coulomb explodes into three singly charged fragments, each captured in coincidence by a velocity map imager which recovers their full three-dimensional (3D) momentum. In this Letter, we provide compelling evidence to suggest that, when ionizing HOD^{2+} (to form HOD^{3+}) at a particular value of Δt, the probe pulse selectively tunnel ionizes along the OH bond in an instance of isotope-selective SFI. See Fig. 1 and Supplemental Material Secs. 1.1 and 1.2 [41] for further experimental details.

*Contact author: phbuck@stanford.edu

Published by the American Physical Society under the terms of the Creative Commons Attribution 4.0 International license. Further distribution of this work must maintain attribution to the author(s) and the published article's title, journal citation, and DOI.

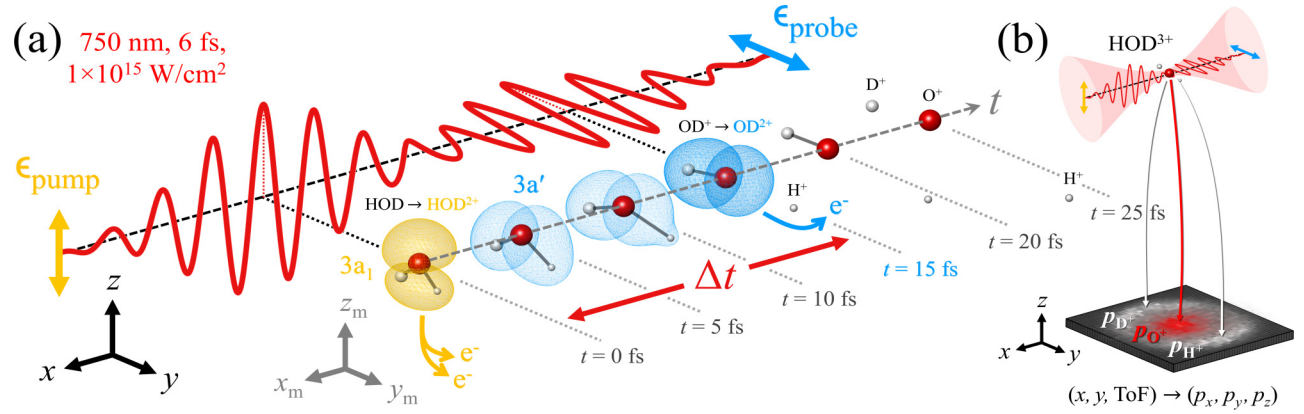


FIG. 1. A schematic of the experiment. (a) Two strong-field cross-polarized pulses, denoted pump and probe, sequentially ionize neutral HOD to form HOD^{2+} and HOD^{3+}, respectively, at an adjustable pump-probe delay (Δt). The pump pulse is polarized along the laboratory-frame z axis and the probe pulse is polarized along the laboratory-frame y axis. After the removal of two electrons from the $3a_1$ molecular orbital of HOD (in yellow), the z_m axis of the resulting dication is preferentially aligned with the laboratory-frame z axis. The dication then evolves over time (t) until the arrival of the probe pulse. If the probe pulse arrives at $t \approx 15$ fs, the molecule undergoes enhanced ionization (EI) in which an electron is removed from the $3a'$ (previously $1b_2$) molecular orbital (in cyan), forming the trication. This occurs preferentially along the OH bond. (b) The trication Coulomb explodes into three ionic fragments ($H^+/D^+/O^+$) which are captured in coincidence by a velocity map imager. The x and y positions of each fragment on the detector are used along with their time-of-flight (ToF) to reconstruct their 3D momentum (p_x, p_y, p_z) upon formation of the trication.

The 3D momentum of each fragment versus pump-probe delay directly reflects the sequential dication and trication dynamics. These data are compared to a detailed *ab initio* model to reconstruct a state-specific "movie" of the interatomic motion in the dication [18,42,43]. This model assumes the pump pulse promotes the Wigner phase-space distribution of the ground vibrational state of the neutral molecule to one of nine dication potential energy surfaces (PESs) with two vacancies in the valence orbitals. This distribution is propagated using 4000 classical trajectories on each of the nine PESs for a time, Δt, before the arrival of the probe pulse. Upon trication formation, the trajectories are propagated under simple Coulomb repulsion of three singly charged fragments, yielding asymptotic fragment momenta for each delay. See Supplemental Material Sec. 2.1 [41] for further details.

Previous work has demonstrated that eliciting EI in D_2O using this cross-polarized pump-probe scheme will preferentially form vacancies in the $3a_1$ valence orbital with the pump pulse [18] and consequently will preselect the particular orientation of the molecule depicted in Fig. 1(a) [19,21]. Removal of an electron from the $3a_1$ valence orbital during the double ionization of D_2O leads to rapid unbending and stretching such that D_2O^{2+} evolves to a favorable geometry for EI in about 20 fs [18]. We find that HOD^{2+} and H_2O^{2+} also display similar enhancements, but at different time delays, and at an appropriate time delay, HOD^{2+} shows evidence for isotope-selective ionization.

The three-body coincidence yield versus pump-probe delay for each isotopologue is displayed in Figs. 2(a)–2(c). A single maximum occurs in each isotopologue with a Gaussian full width at half maximum of about 8 fs (D_2O: 8.6 fs, HOD: 7.7 fs, H_2O: 7.5 fs). The peak enhancement occurs at a delay of 18.4 fs for D_2O, 14.0 fs for HOD, and 13.1 fs for H_2O.

The delayed enhancement for D_2O (compared to H_2O) is consistent with the slower rovibrational dynamics of the OD bond, which should scale as the square root of the reduced mass: $\mu = (m_1 m_2)/(m_1 + m_2)$. Here, $\sqrt{\mu_{OD}/\mu_{OH}} \approx 1.4$. The enhancement in HOD is more complicated: There are *not* two peaks corresponding to the different timescales of the OH and OD bonds. Rather, the enhancement delay is similar to H_2O. These observations point to isotope-selective EI.

The predicted enhancement delay is also plotted in Figs. 2(a)–2(c). This was estimated using a histogram of our simulated trajectories that fulfill the following enhancement criteria: (1) the trajectory is on a PES for a dicationic state with at least one vacancy in the $3a_1$ orbital, and (2) the molecular geometry is in the range of 1.5 Å $< r_{12}$ and $r_{23} <$ 3.5 Å, and $\theta_{123} > 160°$, where r_{12} and r_{23} represent the two bond lengths and θ_{123} represents the bend angle. Good agreement with our measurement suggests that the mechanism for EI, regardless of isotopologue, results from similar orbital vacancies and "critical" geometries.

A representative trajectory is displayed for each isotopologue in Figs. 2(a)–2(c) (i)–(vi). The dynamics in D_2O^{2+} and H_2O^{2+} differ only in speed, both displaying unbending and symmetric stretching that produces a linearized molecule with bond lengths of >2 Å during the peak enhancement. In HOD^{2+}, the hydrogen dissociates promptly but the deuterium remains bound. Consequently, the OD bond never stretches past 2 Å, but oscillates between approximately 0.9 and 1.5 Å with a period of about 20 fs.

The prominence of asymmetric two-body dissociation is seen in Fig. 2(b) (vii), where the momentum of the hydrogen detected in the $H^+/D^+/O^+$ coincidence predominantly asymptotes to about 30 $\hbar/a_0$ at late delays. This is in contrast to the lower momentum asymptote at about 20 $\hbar/a_0$ that results from concerted three-body dissociation. The propensity of HOD^{2+} to dissociate preferentially into H^+/OD^+ has been the subject of many prior studies, both theoretical [43,44] and experimental [45–50].

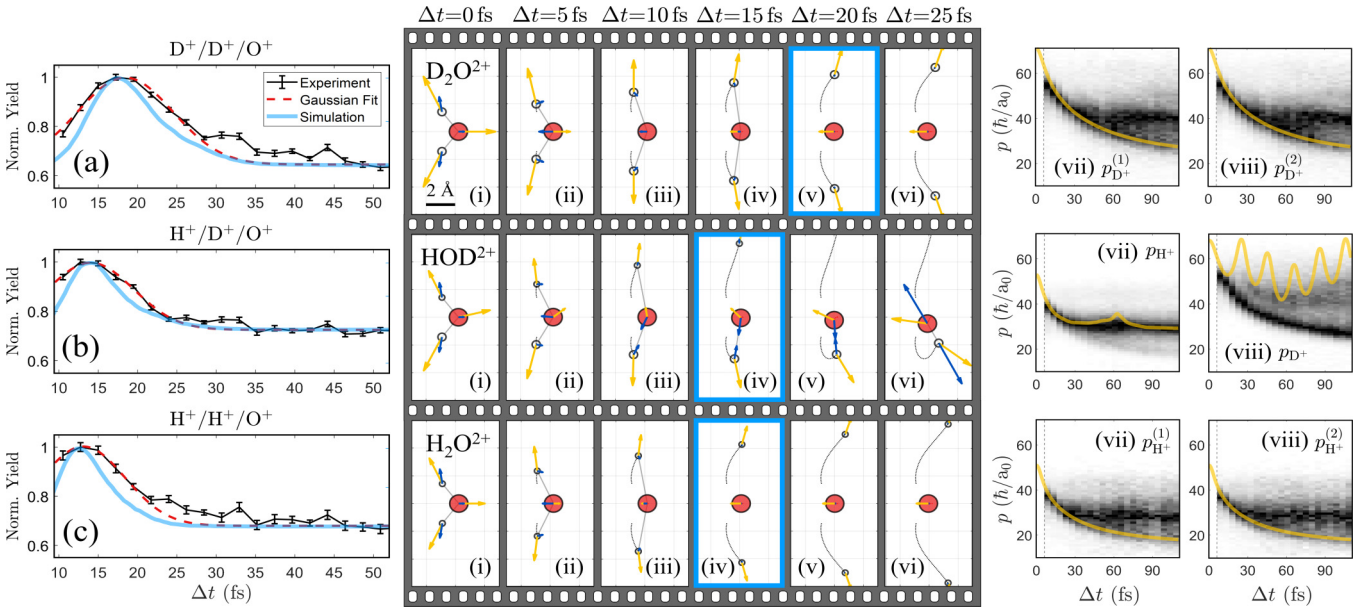


FIG. 2. [(a)–(c)] Solid black line: The yield of the triply charged threefold coincidence channel ($D^+/D^+/O^+$, $H^+/D^+/O^+$, or $H^+/H^+/O^+$) as a function of pump-probe delay Δt (normalized *in situ* by the yield of background N^+ ions). Error bars represent $\sqrt{N}$ noise, where N is the number of coincidences detected. Dotted red line: A Gaussian fit to the early-time experimental data [(a) $\Delta t < 30$ fs, [(b)–(c)] $\Delta t < 21$ fs]. Solid cyan line: A histogram of simulated trajectories that fulfill the EI criteria described in the main text. (a)–(c) (i)–(vi) A series of film-strip plots displaying the instantaneous molecular geometry at various values of Δt for a representative trajectory on the ground state of the dication. The dark blue vectors represent the instantaneous force on each fragment. The yellow vectors represent the asymptotic momentum acquired by each fragment following Coulomb explosion. The cyan borders around select frames represent the approximate times at which the "critical" geometry for EI is reached. (a)–(c) (vii)–(viii) The measured momenta of the hydrogen isotope fragments (each captured in coincidence with the other fragments in their respective threefold coincidence channel) as a function of pump-probe delay. Yellow line: The fragment momenta for the representative trajectory shown in panels (i)–(vi).

The larger stretch of the OH bond greatly affects the measured enhancement. Figures 3(a) and 3(b) show the momentum distribution for triply charged three-body decay of D_2O and HOD at the peak of their respective enhancements. Note the up-down asymmetry of the distribution for HOD^{3+} as compared to D_2O^{3+}. Two separable effects contribute to this asymmetry: First, when experiencing the same forces, the asymptotic momentum of D^+ will be ∼1.4 times larger than H^+ due to the mass disparity. Second, the instantaneous geometry of the molecule is asymmetrically stretched, such that the Coulomb repulsion felt by the D^+ is greater than the repulsion felt by the H^+.

Using our simulated trajectories, we can separate the two effects described above. To do so, we calculate which trajectories best reproduce the experimental momenta of each fragment during the peak of the enhancement. These filtered trajectories are superimposed in cyan in Figs. 3(a) and 3(b). The geometries that correspond to this subset of trajectories are plotted in Figs. 3(c) and 3(d), again in the molecular frame. The weighted mean of these geometries gives us the approximate molecular geometry during the enhancement, plotted as a black circle for each atom in Figs. 3(c) and 3(d). In D_2O: $\langle r_{OD}\rangle = 2.5$ Å, $\langle \theta_{DOD}\rangle = 173°$. In HOD: $\langle r_{OH}\rangle = 2.8$ Å, $\langle r_{OD}\rangle = 1.9$ Å, $\langle \theta_{HOD}\rangle = 169°$. In H_2O: $\langle r_{OH}\rangle = 2.4$ Å, $\langle \theta_{DOD}\rangle = 172°$. Further details can be found in Supplemental Material Sec. 3 [41].

We now consider how the asymmetry in HOD affects the polarization dependence of the enhancement, and compare this case to D_2O. For both isotopologues, we calculate the in-plane angle between the z_m axis and the probe polarization: $\phi = \arctan[(\hat{\epsilon}_{probe}\cdot\hat{y}_m)/(\hat{\epsilon}_{probe}\cdot\hat{z}_m)]$. We then plot the normalized yield versus ϕ as a polar plot in Figs. 3(a)–3(d). Figure 3(d) immediately reveals how the asymmetry in HOD^{2+} affects the enhancement: The distribution peaks when $\hat{\epsilon}_{probe}$ aligns with the OH bond, and not the OD bond. This observation suggests a rare case of bond-selective SFI. During the enhancement, the OH bond is stretched to approximately 2.8 Å whereas the OD is only stretched to 1.9 Å. We posit that this preferential alignment results primarily from a lower tunneling barrier along the OH, as compared to the OD, due to the increased bond distance.

To test our hypothesis, we formed a static tunneling picture. In this picture, at the moment of EI, the instantaneous geometry of the molecule creates a molecular electrostatic potential (MEP) that the electron to be liberated sits in. This potential is deformed linearly by the presence of a strong laser field directed along the molecular axis, forming a tunneling barrier to the continuum. If there is sufficient electron density at the barrier and the barrier is sufficiently small, the electron will tunnel out [22,23]. We simulated the MEP of D_2O^{3+} and HOD^{3+} using a multi-configurational self-consistent field (MCSCF) calculation in GAMESS [51] with a cc-pVTZ Dunning correlation consistent basis set [52]. We used the retrieved molecular geometries reported above, and subjected the molecule to an electric field strength equal to approximately half of our peak field strength $\varepsilon = 0.08\,E_h/ea_0 \sim$

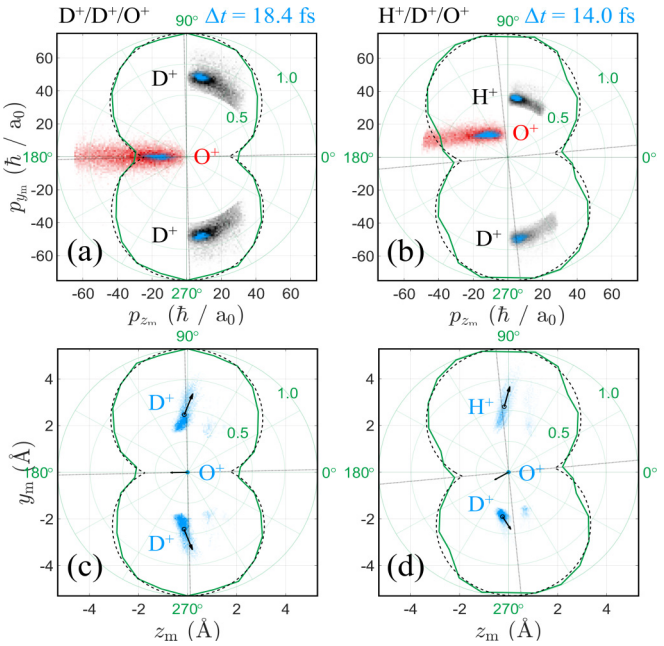


FIG. 3. [(a)–(b)] The retrieved molecular-frame momentum distributions (p_{z_m}, p_{y_m}) for each ion in the $D^+/D^+/O^+$ or $H^+/D^+/O^+$ channel over a 4-fs time window around the maximum enhancement. The hydrogen isotopes are plotted in a black color scale and the oxygen is plotted in a red color scale. Plotted in a cyan color scale are the simulated trajectories that best reproduce the measured momenta within the specified time window. [(c)–(d)] The molecular-frame position-space distributions (z_m, y_m) for the simulated trajectories displayed in (a) and (b), plotted in a cyan color scale. Here, all positions are relative to the position of the oxygen atom. For each ion, the weighted average of the position-space distribution is plotted as a black circle and the weighted average of the velocity distribution is displayed as a black arrow. In (a)–(d), a polar plot is superimposed (in green) representing the normalized yield as a function of the in-plane alignment angle (ϕ) between the probe pulse polarization axis ($\hat{\epsilon}_{\text{probe}}$) and the z_m axis. A cosine fit of ϕ is displayed as a dashed black line, with maxima and minima indicated by dotted black lines.

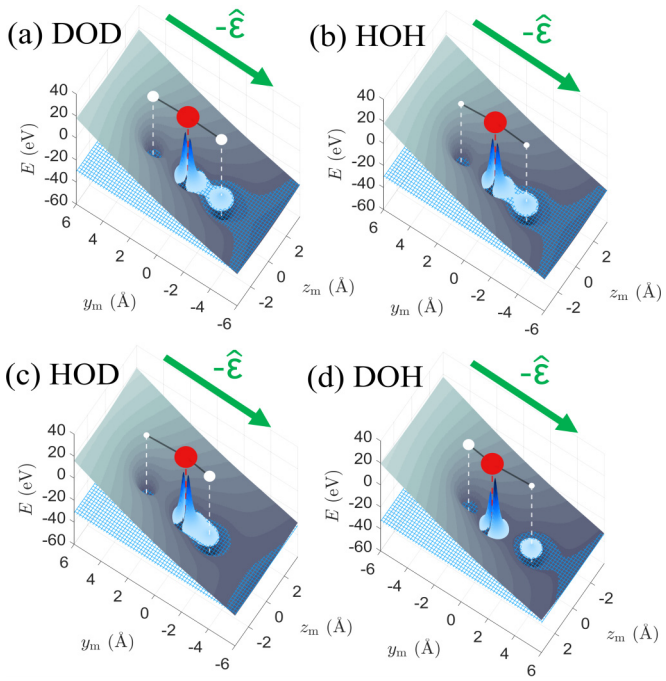


FIG. 4. (a) The molecular electrostatic potential (MEP) of D_2O^{3+} for the retrieved geometry that yielded the maximal enhancement, distorted by a static field ($\varepsilon = 0.08\, E_h/ea_0$) oriented along the y_m axis. The ionization potential (IP) of the distorted $3a'$ (previously $1b_2$) molecular orbital is plotted as a plane with blue grid lines intersecting the MEP at IP $= -30.3$ eV. On top of this plane, the electron density of the $3a'$ orbital is displayed as a surface plot in a cyan color scale. (b) The same as in (a), but for H_2O^{3+} (IP $= -30.6$ eV). (c) The same as in (a) and (b), but for HOD^{3+}, with the static field oriented along the OD bond (IP $= -31.4$ eV). (d) The same as in (a) and (b), but for HOD^{3+} with the static field oriented along the OH bond (IP $= -33.1$ eV).

$\varepsilon_0/2$. From this calculation, we extracted the two-dimensional (2D) MEP of the trication, the 2D electron density of the ionizing orbital in the dication (the $3a'$), and the ionization potential (IP) of the dication.

The static tunneling picture allows for an intuitive visualization of how EI manifests due to a critical geometry. Figures 4(a) and 4(b) display the results for D_2O and H_2O, respectively. In both cases, the presence of a downhill charge lowers both the internal tunneling barrier (formed between the oxygen and the downhill charge) and the external tunneling barrier (formed between the downhill charge and the continuum) below the IP. The lowering of both barriers means that electron density localized at the oxygen can be driven directly out into the continuum.

In order to explain the asymmetrical polarization dependence of EI for HOD, it is instructive to compare the two above cases (D_2O and H_2O) with the case of tunneling along the OD atomic site in HOD, shown in Fig. 4(c). Here, the downhill D lowers the internal tunneling barrier below the IP but not the external barrier at $y_m \approx -3$ Å, which is about 2.5-Å thick. Tunneling along OH is shown in Fig. 4(d). Here, the downhill H^+ lowers the *external* tunneling barrier below the IP, but not the internal tunneling barrier at $y_m \approx 1$ Å, which is only about 0.8-Å thick. Consequently, electron density is trapped on the uphill site behind a thin barrier—ideal conditions for EI. In this circumstance, we should expect tunneling ionization to predominantly occur along the OH bond direction, as opposed to the OD, as observed experimentally. See Supplemental Material Sec. 5 [41] for further analysis.

In summary, through an investigation of enhanced ionization in semiheavy water, we uncovered a unique case in which SFI becomes isotope selective. Using a combination of 3D fragment momentum imaging and *ab initio* theory, we have constructed a time- and state-resolved "molecular movie" of how SFI ultimately favors tunneling along the OH bond. Following double ionization, HOD undergoes asymmetric stretching and unbending due to its mass asymmetry. The hydrogen preferentially dissociates as an H^+ fragment, whereas the deuterium remains trapped within a bound OD^+. The hydrogen therefore explores much larger internuclear distances than does the deuterium. The tunneling barrier for electrons in the $3a'$ molecular orbital (localized on the OD^+ fragment) is significantly lowered by the presence of the

hydrogen at large internuclear distance. Consequently, when a second ionizing pulse encounters this dissociating dication at the right moment in time, one more electron is removed by forming a tunnel along the direction of the dissociating hydrogen. This third ionization event forms OD^{2+}, causing a subsequent Coulomb explosion among the three bodies ($H^+/D^+/O^+$). This isotope-selective ionization phenomenon manifests experimentally in both the timescale and polarization dependence of EI in HOD^{2+} forming HOD^{3+}.

Our measurements suggest that by clever use of EI and isotopic substitution, SFI can be localized along a particular molecular bond, acting as a site-selective probe of charge density. To verify this technique, experiments should be performed on larger selectively deuterated molecules. One such candidate is acetylene (C_2H_2), which has already been demonstrated to exhibit EI [35–37]. Ionization-driven dynamics in HC_2D would foreseeably favor EI along the CH bond. Carrier-envelope phase stabilization and/or simultaneous coincident electron-ion detection may be necessary to measure asymmetric ionization in this case, where the molecule is linear. Extending this experiment to larger molecules may provide a general technique to probe charge density at specific atomic sites within a molecule. For instance, by driving CH stretch in a hydrocarbon where all but one hydrogen has been deuterated and applying a strong field femtoseconds later, one might elicit ionization at the sole carbon site which witnesses the fast CH stretch. As site selectivity in photoionization is usually the purview of XUV/x-ray sources, this technique may enable the use of tabletop IR lasers as a feasible alternative for particular studies of ultrafast charge motion.

A.J.H., M.B., C.C., and P.H.B. were supported by the National Science Foundation. A.J.H. was additionally supported under a Stanford Graduate Fellowship as the 2019 Albion Walter Hewlett Fellow. Work at Lawrence Berkeley National Laboratory (LBNL) was performed under the auspices of the U.S. Department of Energy (DOE), Office of Science, Office of Basic Energy Sciences, Chemical Sciences, Geosciences, and Biosciences Division, under Contract No. DE-AC02-05CH11231, using the National Energy Research Computing Center (NERSC), a DOE Office of Science User Facility, and the Lawrencium computational cluster resource provided by LBNL.

[1] F. Calegari and F. Martin, Open questions in attochemistry, Commun. Chem. **6**, 184 (2023).

[2] H. Johnston, Optics pioneers win Nobel prize, Phys. World **36**, 10 (2023).

[3] M. Ivanov, Concluding remarks: The age of molecular movies, Faraday Discuss. **228**, 622 (2021).

[4] F. Krausz and M. Ivanov, Attosecond physics, Rev. Mod. Phys. **81**, 163 (2009).

[5] L. Young, K. Ueda, M. Gühr, P. H. Bucksbaum, M. Simon, S. Mukamel, N. Rohringer, K. C. Prince, C. Masciovecchio, M. Meyer, A. Rudenko, D. Rolles, C. Bostedt, M. Fuchs, D. A. Reis, R. Santra, H. Kapteyn, M. Murnane, H. Ibrahim, F. Légaré *et al.*, Roadmap of ultrafast x-ray atomic and molecular physics, J. Phys. B: At., Mol. Opt. Phys. **51**, 032003 (2018).

[6] F. Lépine, M. Y. Ivanov, and M. J. J. Vrakking, Attosecond molecular dynamics: Fact or fiction? Nat. Photon. **8**, 195 (2014).

[7] F. Calegari, A. Trabattoni, A. Palacios, D. Ayuso, M. C. Castrovilli, J. B. Greenwood, P. Decleva, F. Martín, and M. Nisoli, Charge migration induced by attosecond pulses in biorelevant molecules, J. Phys. B: At., Mol. Opt. Phys. **49**, 142001 (2016).

[8] J. Li, J. Lu, A. Chew, S. Han, J. Li, Y. Wu, H. Wang, S. Ghimire, and Z. Chang, Attosecond science based on high harmonic generation from gases and solids, Nat. Commun. **11**, 2748 (2020).

[9] P. Walter, T. Osipov, M.-F. Lin, J. Cryan, T. Driver, A. Kamalov, A. Marinelli, J. Robinson, M. H. Seaberg, T. J. A. Wolf, J. Aldrich, N. Brown, E. G. Champenois, X. Cheng, D. Cocco, A. Conder, I. Curiel, A. Egger, J. M. Glownia, P. Heimann, M. Holmes *et al.*, The time-resolved atomic, molecular and optical science instrument at the Linac Coherent Light Source, J. Synchrotron Radiat. **29**, 957 (2022).

[10] M. Rebholz, T. Ding, V. Despré, L. Aufleger, M. Hartmann, K. Meyer, V. Stooß, A. Magunia, D. Wachs, P. Birk, Y. Mi, G. D. Borisova, C. D. C. Castanheira, P. Rupprecht, G. Schmid, K. Schnorr, C. D. Schröter, R. Moshammer, Z.-H. Loh, A. R. Attar *et al.*, All-XUV pump-probe transient absorption spectroscopy of the structural molecular dynamics of di-iodomethane, Phys. Rev. X **11**, 031001 (2021).

[11] N. Berrah, A. Sanchez-Gonzalez, Z. Jurek, R. Obaid, H. Xiong, R. J. Squibb, T. Osipov, A. Lutman, L. Fang, T. Barillot, J. D. Bozek, J. Cryan, T. J. A. Wolf, D. Rolles, R. Coffee, K. Schnorr, S. Augustin, H. Fukuzawa, K. Motomura, N. Niebuhr *et al.*, Femtosecond-resolved observation of the fragmentation of buckminsterfullerene following x-ray multiphoton ionization, Nat. Phys. **15**, 1279 (2019).

[12] C. Cheng, L. J. Frasinski, G. Moğol, F. Allum, A. J. Howard, D. Rolles, P. H. Bucksbaum, M. Brouard, R. Forbes, and T. Weinacht, Multiparticle cumulant mapping for Coulomb explosion imaging, Phys. Rev. Lett. **130**, 093001 (2023).

[13] H. V. S. Lam, A. S. Venkatachalam, S. Bhattacharyya, K. Chen, K. Borne, E. Wang, R. Boll, T. Jahnke, V. Kumarappan, A. Rudenko, and D. Rolles, Differentiating three-dimensional molecular structures using laser-induced Coulomb explosion imaging, Phys. Rev. Lett. **132**, 123201 (2024).

[14] T. Endo, S. P. Neville, V. Wanie, S. Beaulieu, C. Qu, J. Deschamps, P. Lassonde, B. E. Schmidt, H. Fujise, M. Fushitani, A. Hishikawa, P. L. Houston, J. M. Bowman, M. S. Schuurman, F. Légaré, and H. Ibrahim, Capturing roaming molecular fragments in real time, Science **370**, 1072 (2020).

[15] K. Fehre, S. Eckart, M. Kunitski, M. Pitzer, S. Zeller, C. Janke, D. Trabert, J. Rist, M. Weller, A. Hartung, L. P. H. Schmidt, T. Jahnke, R. Berger, R. Dörner, and M. S. Schöffler, Enantioselective fragmentation of an achiral molecule in a strong laser field, Sci. Adv. **5**, eaau7923 (2019).

[16] Z. Vager, R. Naaman, and E. P. Kanter, Coulomb explosion imaging of small molecules, Science **244**, 426 (1989).

[17] H. Stapelfeldt, E. Constant, and P. B. Corkum, Wave packet structure and dynamics measured by Coulomb explosion, Phys. Rev. Lett. **74**, 3780 (1995).

[18] A. J. Howard, M. Britton, Z. L. Streeter, C. Cheng, R. Forbes, J. L. Reynolds, F. Allum, G. A. McCracken, I. Gabalski, R. R. Lucchese, C. W. McCurdy, T. Weinacht, and P. H. Bucksbaum, Filming enhanced ionization in an ultrafast triatomic slingshot, Commun. Chem. **6**, 81 (2023).

[19] A. J. Howard, C. Cheng, R. Forbes, G. A. McCracken, W. H. Mills, V. Makhija, M. Spanner, T. Weinacht, and P. H. Bucksbaum, Strong-field ionization of water: Nuclear dynamics revealed by varying the pulse duration, Phys. Rev. A **103**, 043120 (2021).

[20] C. Cheng, Z. L. Streeter, A. J. Howard, M. Spanner, R. R. Lucchese, C. W. McCurdy, T. Weinacht, P. H. Bucksbaum, and R. Forbes, Strong-field ionization of water. II. Electronic and nuclear dynamics en route to double ionization, Phys. Rev. A **104**, 023108 (2021).

[21] C. Cheng, R. Forbes, A. J. Howard, M. Spanner, P. H. Bucksbaum, and T. Weinacht, Momentum-resolved above-threshold ionization of deuterated water, Phys. Rev. A **102**, 052813 (2020).

[22] T. Zuo and A. D. Bandrauk, Charge-resonance-enhanced ionization of diatomic molecular ions by intense lasers, Phys. Rev. A **52**, R2511 (1995).

[23] T. Seideman, M. Y. Ivanov, and P. B. Corkum, Role of electron localization in intense-field molecular ionization, Phys. Rev. Lett. **75**, 2819 (1995).

[24] C. Trump, H. Rottke, M. Wittmann, G. Korn, W. Sandner, M. Lein, and V. Engel, Pulse-width and isotope effects in femtosecond-pulse strong-field dissociation of H_2^+ and D_2^+, Phys. Rev. A **62**, 063402 (2000).

[25] F. Légaré, I. V. Litvinyuk, P. W. Dooley, F. Quéré, A. D. Bandrauk, D. M. Villeneuve, and P. B. Corkum, Time-resolved double ionization with few cycle laser pulses, Phys. Rev. Lett. **91**, 093002 (2003).

[26] T. Ergler, A. Rudenko, B. Feuerstein, K. Zrost, C. D. Schröter, R. Moshammer, and J. Ullrich, Time-resolved imaging and manipulation of H_2 fragmentation in intense laser fields, Phys. Rev. Lett. **95**, 093001 (2005).

[27] I. Ben-Itzhak, P. Q. Wang, A. M. Sayler, K. D. Carnes, M. Leonard, B. D. Esry, A. S. Alnaser, B. Ulrich, X. M. Tong, I. V. Litvinyuk, C. M. Maharjan, P. Ranitovic, T. Osipov, S. Ghimire, Z. Chang, and C. L. Cocke, Elusive enhanced ionization structure for H_2^+ in intense ultrashort laser pulses, Phys. Rev. A **78**, 063419 (2008).

[28] H. Xu, F. He, D. Kielpinski, R. Sang, and I. Litvinyuk, Experimental observation of the elusive double-peak structure in R-dependent strong-field ionization rate of H_2^+, Sci. Rep. **5**, 13527 (2015).

[29] F. Légaré, K. F. Lee, I. V. Litvinyuk, P. W. Dooley, S. S. Wesolowski, P. R. Bunker, P. Dombi, F. Krausz, A. D. Bandrauk, D. M. Villeneuve, and P. B. Corkum, Laser Coulomb-explosion imaging of small molecules, Phys. Rev. A **71**, 013415 (2005).

[30] H. Liu, M. Li, X.-G. Xie, C. Wu, Y.-K. Deng, C.-Y. Wu, Q.-H. Gong, and Y.-Q. Liu, Charge resonance enhanced multiple ionization of H_2O molecules in intense laser fields, Chin. Phys. Lett. **32**, 063301 (2015).

[31] G. A. McCracken, A. Kaldun, C. Liekhus-Schmaltz, and P. H. Bucksbaum, Geometric dependence of strong field enhanced ionization in D_2O, J. Chem. Phys. **147**, 124308 (2017).

[32] J. P. Brichta, S. J. Walker, R. Helsten, and J. H. Sanderson, Ultrafast imaging of multielectronic dissociative ionization of CO_2 in an intense laser field, J. Phys. B: At., Mol. Opt. Phys. **40**, 117 (2007).

[33] I. Bocharova, R. Karimi, E. F. Penka, J.-P. Brichta, P. Lassonde, X. Fu, J.-C. Kieffer, A. D. Bandrauk, I. Litvinyuk, J. Sanderson, and F. Légaré, Charge resonance enhanced ionization of CO_2 probed by laser Coulomb explosion imaging, Phys. Rev. Lett. **107**, 063201 (2011).

[34] P. Song, Y. Zhu, Y. Yang, X. Wang, C. Meng, J. Zhao, J. Liu, Z. Lv, D. Zhang, Z. Zhao, and J. Yuan, Dissociative multiple ionization of carbon dioxide dimers in intense femtosecond laser fields, Phys. Rev. A **106**, 023109 (2022).

[35] X. Gong, Q. Song, Q. Ji, H. Pan, J. Ding, J. Wu, and H. Zeng, Strong-field dissociative double ionization of acetylene, Phys. Rev. Lett. **112**, 243001 (2014).

[36] S. Erattupuzha, C. L. Covington, A. Russakoff, E. Lötstedt, S. Larimian, V. Hanus, S. Bubin, M. Koch, S. Gräfe, A. Baltuška, X. Xie, K. Yamanouchi, K. Varga, and M. Kitzler, Enhanced ionisation of polyatomic molecules in intense laser pulses is due to energy upshift and field coupling of multiple orbitals, J. Phys. B: At., Mol. Opt. Phys. **50**, 125601 (2017).

[37] C. Burger, A. Atia-Tul-Noor, T. Schnappinger, H. Xu, P. Rosenberger, N. Haram, S. Beaulieu, F. Légaré, A. S. Alnaser, R. Moshammer, R. T. Sang, B. Bergues, M. S. Schuurman, R. De Vivie-Riedle, I. V. Litvinyuk, and M. F. Kling, Time-resolved nuclear dynamics in bound and dissociating acetylene, Struct. Dyn. **5**, 044302 (2018).

[38] J. L. Holmes, K. J. Jobst, and J. K. Terlouw, Isotopic labelling in mass spectrometry as a tool for studying reaction mechanisms of ion dissociations, J. Labelled Compd. Radiopharm. **50**, 1115 (2007).

[39] B. R. Heazlewood, A. T. Maccarone, D. U. Andrews, D. L. Osborn, L. B. Harding, S. J. Klippenstein, M. J. T. Jordan, and S. H. Kable, Near-threshold H/D exchange in CD_3CHO photodissociation, Nat. Chem. **3**, 443 (2011).

[40] T. Severt, E. Weckwerth, B. Kaderiya, P. Feizollah, B. Jochim, K. Borne, F. Ziaee, Kanaka Raju P, K. D. Carnes, M. Dantus, D. Rolles, A. Rudenko, E. Wells, and I. Ben-Itzhak, Initial-site characterization of hydrogen migration following strong-field double-ionization of ethanol, Nat. Commun. **15**, 74 (2024).

[41] See Supplemental Material at http://link.aps.org/supplemental/10.1103/PhysRevResearch.7.L012062 for more information on (1) how the strong-field pulse pairs were generated, (2) the coincident ion detection scheme, (3) how the molecular frame was experimentally retrieved, (4) how the dication dynamics were modeled, (5) the measurement of the triply-charged three-body dissociations, (6) how the static tunneling picture informs the degree of enhancement measured for each isotopologue.

[42] Z. L. Streeter, F. L. Yip, R. R. Lucchese, B. Gervais, T. N. Rescigno, and C. W. McCurdy, Dissociation dynamics of the water dication following one-photon double ionization. I. Theory, Phys. Rev. A **98**, 053429 (2018).

[43] B. Gervais, E. Giglio, L. Adoui, A. Cassimi, D. Duflot, and M. E. Galassi, The H_2O^{2+} potential energy surfaces dissociating into H^+/OH^+: Theoretical analysis of the isotopic effect, J. Chem. Phys. **131**, 024302 (2009).

[44] D. Dey and A. K. Tiwari, Effect of vibrational pre-excitation on the dissociation dynamics of HOD^{2+}, J. Phys. Chem. A **120**, 2629 (2016).

[45] P. J. Richardson, J. H. D. Eland, P. G. Fournier, and D. L. Cooper, Spectrum and decay of the doubly charged water ion, J. Chem. Phys. **84**, 3189 (1986).

[46] S. Legendre, E. Giglio, M. Tarisien, A. Cassimi, B. Gervais, and L. Adoui, Isotopic effects in water dication fragmentation, J. Phys. B: At., Mol. Opt. Phys. **38**, L233 (2005).

[47] A. M. Sayler, M. Leonard, K. D. Carnes, R. Cabrera-Trujillo, B. D. Esry, and I. Ben-Itzhak, Preference for breaking the O–H bond over the O–D bond following HDO ionization by fast ions, J. Phys. B: At., Mol. Opt. Phys. **39**, 1701 (2006).

[48] D. Mathur, K. Dota, D. Dey, A. K. Tiwari, J. A. Dharmadhikari, A. K. Dharmadhikari, S. De, and P. Vasa, Selective breaking of bonds in water with intense, 2-cycle, infrared laser pulses, J. Chem. Phys. **143**, 244310 (2015).

[49] T. Jahnke, R. Guillemin, L. Inhester, S.-K. Son, G. Kastirke, M. Ilchen, J. Rist, D. Trabert, N. Melzer, N. Anders, T. Mazza, R. Boll, A. De Fanis, V. Music, T. Weber, M. Weller, S. Eckart, K. Fehre, S. Grundmann *et al.*, Inner-shell-ionization-induced femtosecond structural dynamics of water molecules imaged at an x-ray free-electron laser, Phys. Rev. X **11**, 041044 (2021).

[50] R. Guillemin, L. Inhester, M. Ilchen, T. Mazza, R. Boll, T. Weber, S. Eckart, P. Grychtol, N. Rennhack, T. Marchenko, N. Velasquez, O. Travnikova, I. Ismail, J. Niskanen, E. Kukk, F. Trinter, M. Gisselbrecht, R. Feifel, G. Sansone, D. Rolles *et al.*, Isotope effects in dynamics of water isotopologues induced by core ionization at an x-ray free-electron laser, Struct. Dyn. **10**, 054302 (2023).

[51] G. M. J. Barca, C. Bertoni, L. Carrington, D. Datta, N. De Silva, J. E. Deustua, D. G. Fedorov, J. R. Gour, A. O. Gunina, E. Guidez, T. Harville, S. Irle, J. Ivanic, K. Kowalski, S. S. Leang, H. Li, W. Li, J. J. Lutz, I. Magoulas, J. Mato, V. Mironov *et al.*, Recent developments in the general atomic and molecular electronic structure system, J. Chem. Phys. **152**, 154102 (2020).

[52] T. H. Dunning Jr., Gaussian basis sets for use in correlated molecular calculations. I. The atoms boron through neon and hydrogen, J. Chem. Phys. **90**, 1007 (1989).